4

Electrochemically deposited bimetallic nanoparticles as a SERS platform and its application for trace detection of antibiotics in farm eggs

In this chapter, the working of an electrochemically fabricated SERS substrate is presented. The proposed SERS substrate has been obtained by depositing bimetallic copper-gold nanoparticles through electrochemical technique on indium tin oxide glass. The applicability of the designed SERS platform has been demonstrated through the detection of two important antibiotics, SFZ and TCH, commonly employed in egg farms. Additionally, to enhance the analytical capabilities, a ML-based model was employed in conjunction with PCA as a dimensionality reduction technique. This integrated approach allows for an effective classification of targeted analytes present in egg samples.

4.1 Introduction

Maintaining precise control over the surface morphology of nanostructures is critical for fabricating a highly sensitive and reproducible SERS substrate. A primary issue with traditional deposition methods like drop casting is the inconsistency in the deposition of nanostructures, resulting in the fluctuations in Raman band intensities. Amongst the various methods available for depositing metal nanoparticles on glass substrates, ED stands out as a versatile technique for large-scale fabrication of nanoparticles over conducting glass surfaces. This deposition process involves nucleation and growth mechanisms [1]. The surface morphology of metal nanostructures significantly influences the enhancement of Raman bands of the target analyte. To fabricate three-dimensional nanostructures using ED, a slow growth process is necessary. Although Au and Ag are commonly used noble metals for fabrication of SERS

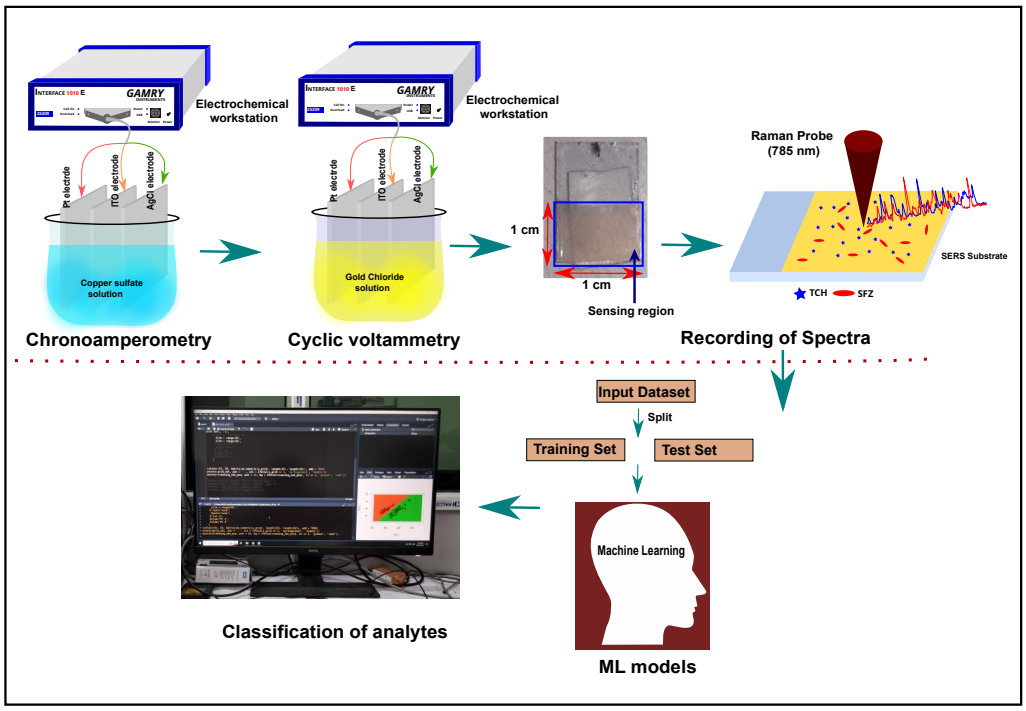

Figure 4.1: Schematic representation of the workflow of the proposed sensing scheme

substrates, Cu-based substrates are gaining popularity due to their abundance and relatively low-cost [2–5]. However, Cu-based substrates are susceptible to oxidation, leading to a rapid deterioration of the plasmon resonance condition. This can be obviated by employing bimetallic systems such as Ag or Au [6]. In the case of Cu, interference from interband transitions poses challenges for plasmonic sensing below the incident wavelength of 600 nm [7].

In this chapter the fabrication of a bimetallic Cu-AuNPs on ITO as a sensitive SERS platform is presented. The schematic of the proposed sensing methodology is depicted in figure 4.1. The fabrication process involves electrochemical deposition of copper CuNPs onto a ITO glass substrate using CA technique. In CA, the current response evolves over time while maintaining potentiostatic control of the system. The working electrode shifts from a potential devoid of electrode reactions to a level corresponding to the mass-transport limited current, and the resulting transient current-time profile is recorded [8]. Subsequently, AuNPs were deposited using CV technique. In CV, the morphology of the deposited nanoparticles is controlled by varying the applied voltage. By carefully adjusting the applied voltage between the range of -0.2 V to +1.1 V, a uniform deposition of AuNPs on Cu-coated ITO glass substrate has been achieved.

The nanostructure thus, formed by this technique with optimized control parameters enhances the Raman bands upto $\sim 10^7$ with a good uniformity characteristic over the sensing region of the substrate. The density of the AuNPs deposited over the Cu-ITO glass substrate can be varied by changing the number of deposition cy-

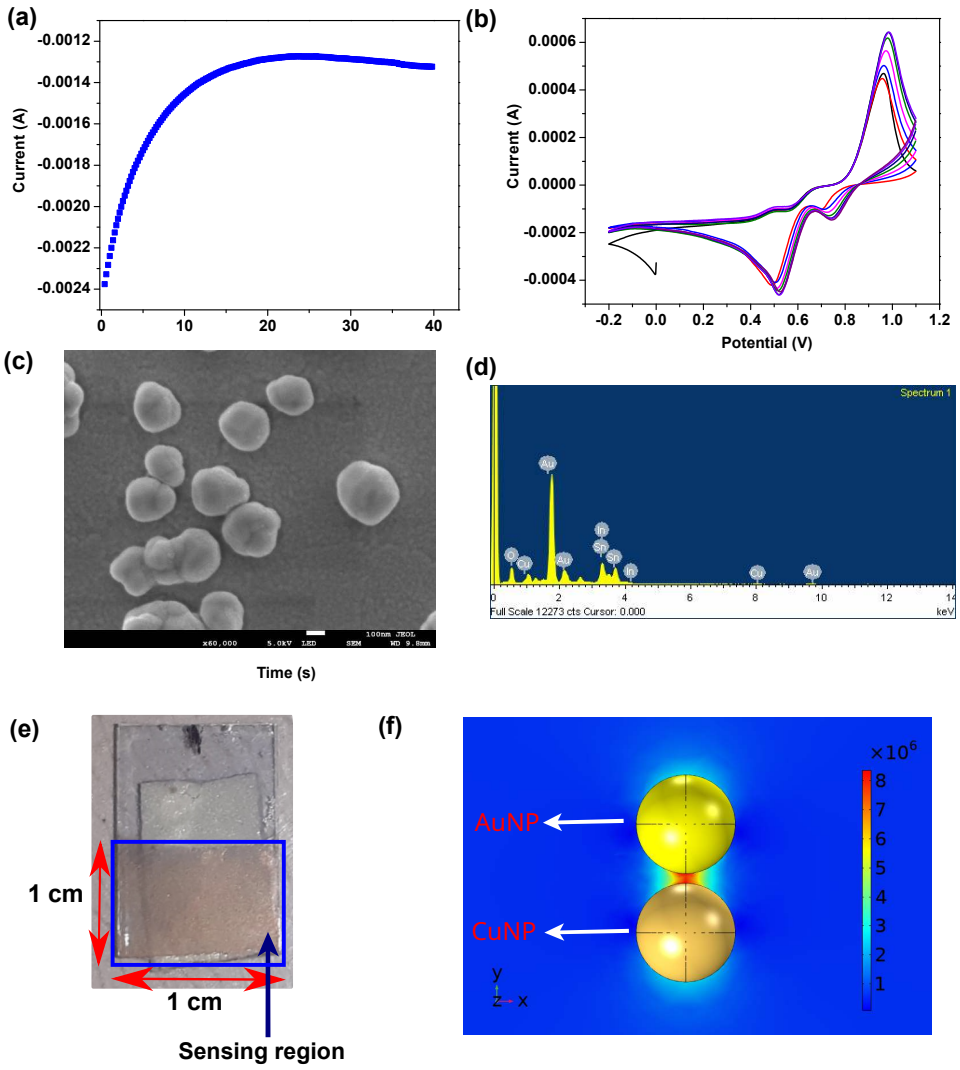

Figure 4.2: (a) FESEM image of the fabricated SERS substrate (b) EDX image showing the elements present in the designed SERS substrate (c) CA plot of the ED of Cu over ITO glass substrate (d) CV plot of the electrochemical deposition of gold layer over the ITO glass for 7 consecutive cycles. (e) Image of the fabricated SERS substrate (f) COMSOL multiphysics simulation image depicting the coupled EM field amplitude in the hotspot region of the SERS substrate; incident electric field amplitude was assumed as 6.18×10^4 Vm^{-1}

cles. The deposition was performed using low precursor concentration without any surfactant at room temperature. Among the various deposition cycles, seven cycle of ED yields the best SERS performance in terms of average enhancement factor and the uniformity characteristic of the substrate. Although bimetallic nanoparticles based SERS substrates have been previously reported [6, 9–11], the present work reports a detailed deposition condition parameters to be maintained to obtain an optimized SERS performance on the proposed platform. Furthermore, ML technique was integrated to classify the target specimens through training and analyzing dataset enabling identification of the target samples easily and more accurately. Prior to implement the ML, PCA of the spectral data of the targeted samples was computed. PCA is an unsupervised dimensionality reduction approach that converts the input

dataset orthogonally into a small subspace of features [12]. SVM, KSVM, Naive Bayes, and KNN algorithms were initially implemented to validate the ML-based classification. SVM is a ML technique for classifying the dataset and analyzing the regression patterns. It selects the hyperplane to maximize the class separation and reduce misclassifications. The KSVM is a non-linear SVM model which uses the radial kernel function [13, 14]. Naive Bayes algorithm is a supervised ML technique based on Bayes theorem [15] for the classification of the groups. KNN is a nonlinear classifier technique that compares the distance between the unknown and known examples to achieve the required classification [12]. In the present work, it has been observed that the KNN technique combining with the PCA yields a classification accuracy of 94%.

4.2 Materials and methods

4.2.1 Chemicals

$HAuCl_4 \cdot 3\,H_2O$, acetonitrile, potassium chloride (KCl) and ethylenediaminetetraacetic acid disodium salt dihydrate (Na_2EDTA) were obtained from Merck, India, while R6G and MG were procured from Alpha Aesar, India. SFZ ($C_{10}H_{11}N_3O_3S$) and TCH ($C_{22}H_{24}N_2O_8 \cdot HCl$) were acquired from a nearby pharmaceutical supplier. ITO glass sheets were purchased from a local vendor. All chemicals were utilized as received without any additional treatment.

4.2.2 Fabrication of Cu-ITO glass SERS substrate

CuNPs were fabricated on ITO glass using the CA deposition method with a slight modification reported elsewhere [16]. For ED of Cu onto the ITO surface, 0.1 M aqueous solution of $CuSO_4$ was prepared in the lab. Deposition was performed in a three-electrode system, a constant dc bias potential of -0.9 V was maintained to deposit CuNPs onto the working electrode (ITO). At -0.9 V dc bias potential, copper ions in the solution underwent reduction, leading to the formation of nanoparticles on the ITO substrate surface. Figure 4.2(a) depicts the characteristic deposition curve of CA which clearly shows that the deposition current increases with the reaction time. After 17 s, the system reaches a plateau indicating the attainment of a steady state.

4.2.3 Fabrication of Cu-Au-ITO glass SERS substrate

The ED of AuNPs over the Cu-ITO glass substrate was performed in a three-electrode setup where a conducting Cu-ITO glass was used as a working electrode. A platinum

wire (Pt) and a Ag/AgCl electrode were used as the reference and counter electrodes, respectively. 5 mM solution of $HAuCl_4 \cdot 3\,H_2O$ was prepared in 0.1 M KCl solution. The CV was carried out at a scan rate of 20 mVs^{-1} in the potential range of 0.2 V to +1.1 V. The appearance of a light pink-colored film over the ITO glass surface indicates the deposition of AuNPs over the substrate. Figure 4.2(b) depicts the deposition curve of AuNPs. The cathode peaks appearing at 0.75 V and 0.5 V are attributed to the reduction reactions of Au^{3+} to Au^{1+} and Au^{1+} to Au^0, respectively. The sharp anodic peak appearing at +0.92 V resembles Cl^- to $\frac{1}{2}$ Cl_2 oxidation process. The increase in the area under the CV curve after each cycle indicates the deposition of multiple AuNPs layers over the Cu-ITO glass substrate. Here, we have captured the CV responses in the potential range between 0.2 V and +1.1 V. Below 0.2 V, no reduction activity was monitored and above +1.1 V, there would be a possibility of splitting water molecules in the aqueous electrolyte. With increasing number of CV cycles, the average dimension of the deposited nanoparticles will increase and then would affect the performance of the designed SERS substrate. In the present study, it has been observed that beyond 7 CV cycles, the AuNPs loading over the ITO glass substrate is increased significantly and thus, causes the formation of nanoclusters. The SERS performance in terms of the average enhancement factor starts degrading beyond this cycle. Table 4.1 shows the comparison of the average EF values, when different cycles of depositions were considered to fabricate the proposed SERS substrate.

Table 4.1: Comparison of the SERS performance with the number of CV cycles

No of CV cycles	Voltage range	EF	Comment
1	−0.2 to +1.1 V	No SERS effect	No observable Au deposition
2			
3		10^2	Observable SERS results
4		10^3	
5		10^4	
6		10^4	
7		10^7	Highest EF was observed
8		10^5	Decrease in SERS performance
9		10^3	
10		10^3	

As the number of CV deposition cycles increases, more material is deposited on the surface of the electrode, typically resulting in a thicker film. The thickness of the deposited metal will tend to increase with more cycles. Since SERS is a surface phenomena, the nanostructures on the surface primarily contributes to the scattered SERS signal intensity. After 7 cycles, the deposited metal layer reach a critical thickness beyond which the SERS performance degrades. This has attributed to the factors such as reduced surface area and increased resistance. The excessive deposition can lead to a reduction in active surface area, as the layer becomes more

uniform. Also, thick layers may introduce resistive pathways reducing the efficiency of electron transfer. Figure 4.2 (c) shows the FESEM image of the deposited bimetallic nanoparticles over the ITO substrate. Figure 4.2(d) shows the EDX spectra of the proposed SERS platform that indicates the presence of different elements on the ITO substrate. Again figure 4.2(e) depicts the image of the fabricated SERS substrate.

4.2.4 Sample preparation

To isolate the targeted antibiotics from the egg samples, a slightly different approach was implemented compared to the technique described by Wang et al. [17]. Six fresh whole eggs were homogenized at room temperature and stored at 4 °C until extraction. Two grams of homogenized egg sample was weighed into a 50 mL centrifuge tube, and 20 µL of the working standard solution was added to prepare the solution. Additionally, the sample was vortexed for 30 s, and the tube was left at room temperature for 2 h. Subsequently, 7.5 mL of a 90:10 (v/v) acetonitrile and water mixture, along with 0.5 $molL^{-1}$ of Na_2EDTA solutions, was added to the sample. The sample was then centrifuged at 6000 rpm for 10 min at 4 °C, and the supernatant was obtained.

4.2.5 Raman instrumentation and data analysis

The specification of the Raman instrument is described in section 2.2.4. R data analysis software was used for the data analysis. ML and PCA models were developed from R standard libraries [18]. For ML classification, 200 different farm egg samples were collected and extracted by using the protocol described in the section 4.2.4.

4.2.6 Acquisition of spectra

20 µL of the analyte sample was dispensed over the sensing region of the proposed SERS substrates. Upon vacuum drying for 1 h, the SERS spectra of the samples were recorded for five consecutive times. For the field-collected egg sample, 20 µL of the extracted sample was dispensed and then dried for 5 h in a vacuum desiccator prior to perform the SERS investigations.

4.2.7 EM simulation

To evaluate the amplitude of coupled EM field in the hotspot regions of the SERS substrate, EM simulation was performed. Wave optics module from COMSOL multiphysics 5.2 simulation tool was used for the present study. The simulation was performed for three different combinations of nanoparticles viz AuNP-AuNP, CuNP-AuNP, and CuNP-CuNP, respectively. To reduce the processing time, the simulation

study was performed for two nanoparticles of size 100 nm separated by a distance of 5 nm. The coupled EM field amplitude near the hotspot regions of the SERS substrate is shown in figure 4.2(f). The incident electric field amplitude was assumed as 6.18×10^4 Vm^{-1}. The simulation studies reveal that for the considered CuNP-AuNP over the ITO glass, the maximum coupled EM field amplitude was found to be 8.2×10^6 Vm^{-1} in the hotspot regions when the substrate was illuminated with a 785 nm laser. The details of EF, estimated through both simulation and experimental methods, are described in table 8.16.

4.2.8 XPS and XRD characterization of the Cu-Au-ITO platform

The XPS analysis has been carried out to confirm the presence of Au, Cu in the fabricated SERS platform. The XPS analysis reveals the concentration of Au, Cu, and C in the fabricated SERS substrate and amounts are found to be 6.87%, 1%, 52.02%, respectively. Figure 4.3 depicts the survey scan of the fabricated SERS substrate, the peaks near 87 eV, 283 eV, and 933 eV confirm the presence of Au, C, and Cu in the designed SERS substrate.

Figure 4.3(b)-(d) represents the high-resolution XPS spectra of Au 4f, C 1s, and Cu 2p, respectively. In figure 4.3, two prominent peaks have been observed at 83.9 eV and 87.5 eV which correspond to the $Au^4f_{7/2}$ and $Au^4f_{5/2}$, respectively. These data confirm the presence of Au in the designed SERS substrate. In figure 4.3(c), three peaks appearing at 285.8 eV, 286 eV, and 288.5 eV confirm the presence of C 1s C−C, C 1s C−O, and C−1 s O−C=O of the fabricated SERS substrate. The two peaks shown in figure 4.3(d) near 931.0 eV and 950.8 eV are attributed to $Cu^2p_{3/2}$ and $Cu^2p_{1/2}$, respectively. Figure 4.3(e) depicts the XRD analysis of the designed Cu-Au-ITO SERS platform. The XRD peaks near 2 ϑ= 37.4 are due to the Bragg reflections of Au (111) and Cu (0,0,2). The peak at 2ϑ= 43.5 corresponds to the Au (2,0,0) and Cu (1,1,1) planes; the XRD peak at 2ϑ= 64.1 is due to the Au (2,2,0) plane and the peak near 77.05 are due to the Au (3,1,1) and Cu (2,0,0), respectively. The XRD data reveal the presence of gold and copper crystal structure in the fabricated substrate.

4.3 Results and discussion

4.3.1 Optimization of the SERS substrate

The SERS performance of the designed SERS substrates was evaluated for three different situations - CuNPs on ITO, AuNPs on ITO, and the bimetallic Cu-AuNPs on

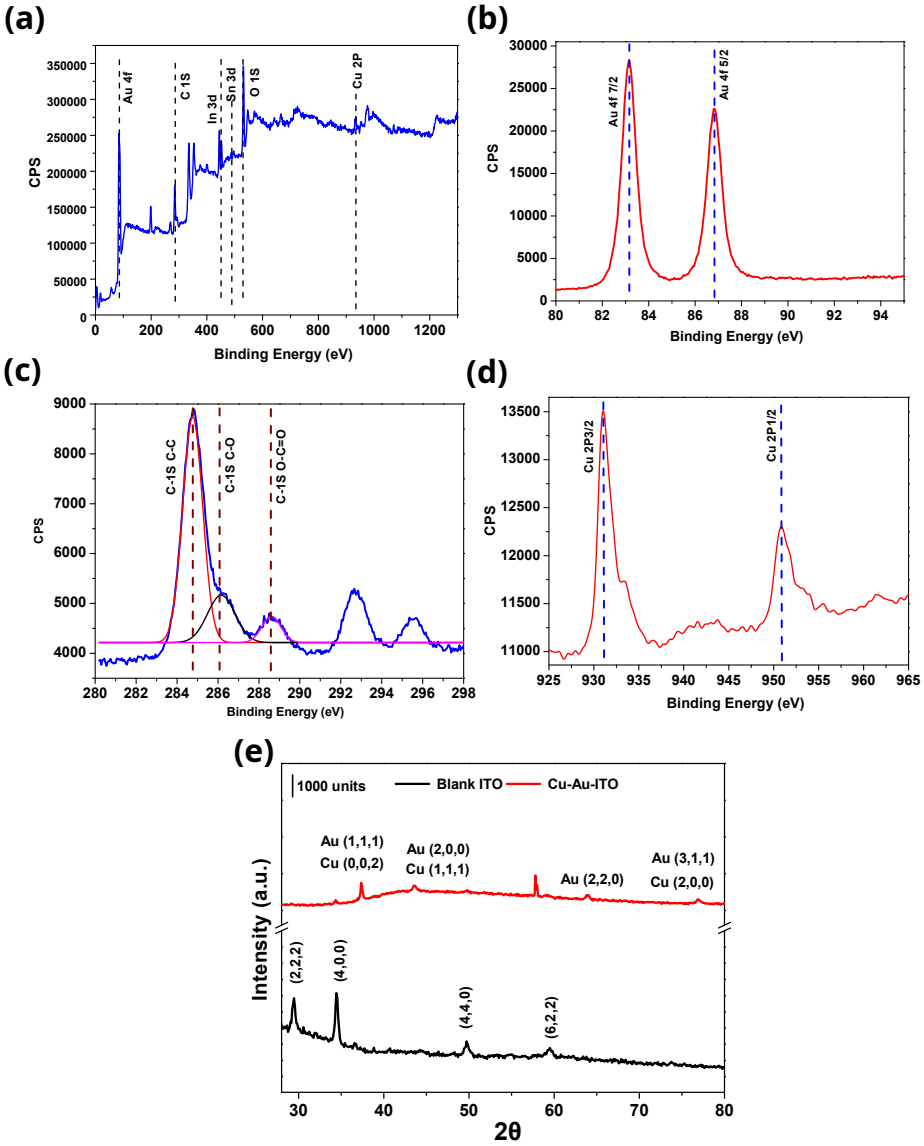

Figure 4.3: (a) XPS survey scan of the fabricated SERS substrate. High resolution XPS spectra for (b) AuNP, (c) carbon, (d) copper, and (e) XRD characterization of fabricated Au-Cu-ITO platform

ITO substrate taking MG as a test analyte. Figure 4.4(a) shows the characteristic SERS spectra of MG while considering these three different situations. The figure clearly shows that for Cu-AuNPs on ITO, the designed SERS substrate yields the highest SERS signal intensities compared to the other two substrates. This enhancement in the SERS performance is attributed to the bimetallic contribution the LSPR effect, which would contributes to the overall enhancement of the coupled electromagnetic field and as a result to the SERS signal intensities.

The performance of the proposed SERS platform was realized with the standard Raman active samples - MG and R6G. For both MG and R6G, first a stock solution of 1 µM was prepared by dissolving the specific amount of sample in DI water. Both the stock samples were then diluted with DI water to obtain other lower concentrated

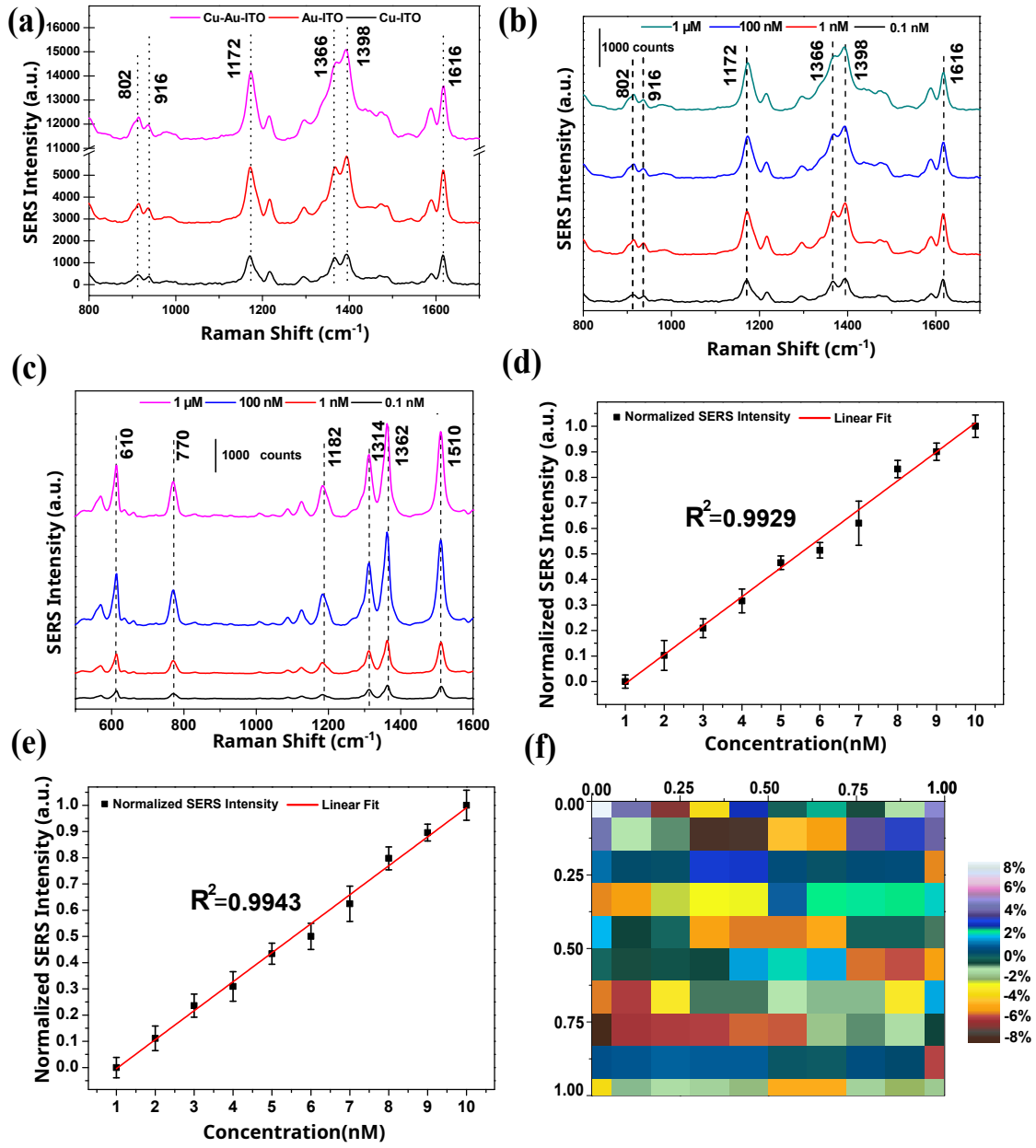

Figure 4.4: (a) Comparison of the SERS performance of the Cu-ITO, Au-ITO, and the Cu-Au-ITO SERS platform taking MG as a test analyte.(b) SERS spectra recorded on Cu-Au-ITO glass SERS substrate for variation of concentration of MG. (c) SERS spectra recorded on Cu-Au-ITO glass SERS substrate for variation of concentration of R6G. (d) Variation of the normalized Raman signal intensity with the variation of concentration of MG for the Raman band near 1172 cm^{-1}. (e) Variation of the normalized Raman signal intensity with the variation concentration of R6G for the Raman band near 1362 cm^{-1}. (f) Raman mapping of the SERS substrate for the signature Raman peak 1172 cm^{-1} of MG over an array 10 × 10; (Error bars are plotted using the standard deviation, calculated from five repetitions for each sample)

samples. Following the sample preparation step, the SERS spectra were recorded from the designed Cu-AuNPs on ITO platform. Figure 4.4(b) and (c) depicts the recorded SERS spectra of MG and R6G, respectively in the concentration range 0.1 nM - 1 µM. The characteristic spectra clearly indicate that with the present Cu-Au-ITO glass based SERS substrate, concentration down to 0.1 nM can be easily detected. The characteristic Raman bands for MG and R6G are illuminated in appendix section (table 8.1 and table 8.2). The linear regression analysis for both the samples MG and R6G was carried out and the results are shown in figure 4.4(d) and (e), respectively. The inset curve in figure 4.4(d) represents the variations of SERS signal intensities of MG in the concentration range 0.1 to 1 nM. The coefficient of linear regression (R^2) values for MG and R6G were found to be 0.9929 and 0.9943, respectively, suggesting a good degree of correlation between the analytes concentrations and the intensities of scattered Raman signals from the sensing region of the substrate. The uniformity of the designed SERS platform was evaluated by mapping the signature Raman peak of MG at 1398 cm^{-1} over a sensing area of 1 mm^2. Figure 4.4 illustrates the mapping characteristic for MG and a maximum fluctuations of 8% was observed from its average signal intensity.

4.3.2 Estimation of LoD

In order to calculate the LoD, the concentration range of 0.1 nM to 10 nM was considered. From figure 4.4(d), the LoD was calculated using the equation 2.1. For MG, the LoD of the proposed SERS platform was estimated to be 0.75 nM.

4.3.3 Precision evaluation of the SERS substrate

The precision of the designed SERS substrate has been demonstrated through the repeatability study. The repeatability of the present sensing scheme is realised through detection of SERS signals for ten consecutive times of the same sample. For this, 1 µM of the analytes of MG and R6G were dispensed over the sensing region of the SERS substrate and the scattered Raman signals were recorded. Figure 4.5 depicts the repeatability study of the SERS substrate and the maximum RSD for both the analytes are found to be 6%. The low RSD values represent that the fabricated SERS substrate is highly precise in nature.

4.3.4 Evaluation of temporal evaluation and reproducibility characteristics

In the next step, the temporal evaluation of the designed SERS platform was performed. The scattered Raman signal intensity variations were studied with the time

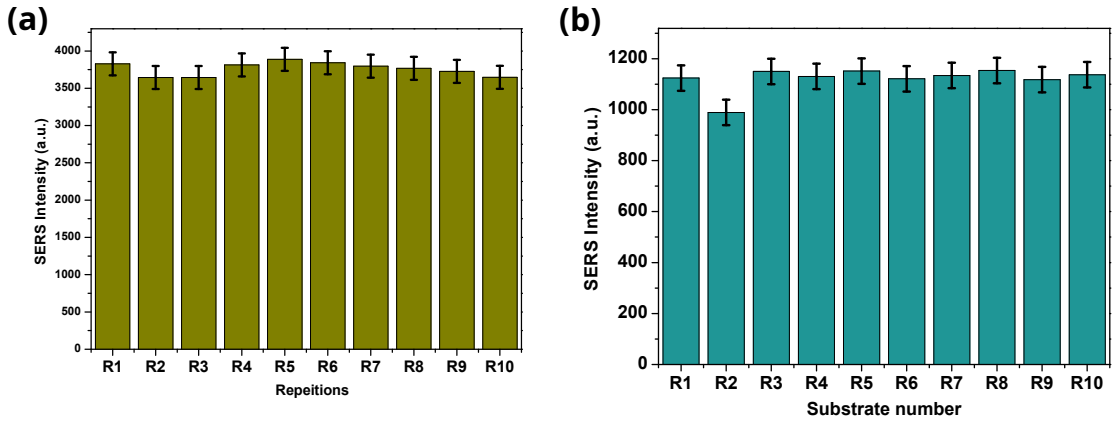

Figure 4.5: Repeatability study for 10 different repetitions for the characteristics Raman peak (a) MG at 1172 cm^{-1} (b) 1362 cm^{-1} (Error bars are plotted using the standard deviation, calculated from five repetitions for each sample)

taking MG as an analyte. Figure 4.6(a) shows the variations of the SERS signal intensities recorded by the spectrometer for 22 consecutive days. The signature Raman bands of MG near 1172 cm^{-1}, 1398 cm^{-1}, and 1618 cm^{-1} have been considered to evaluate the temporal performance of the proposed SERS substrate. The figure 4.6(a) shows that the signal intensities are reasonably stable up to first 20 days, and after that it started to attenuate gradually which suggest a good temporal stability of the proposed sensing platform.

The reproducibility characteristics of the proposed bimetallic SERS substrate were evaluated for ten identical substrates using MG and R6G as the target analytes. For this, 10 µL of 1 µM concentrations of each sample was dispensed over the sensing region of the proposed substrates. The scattered Raman signals were recorded from five random locations for each substrate. Figure 4.6(b) and (c) shows the reproducibility characteristics of the proposed SERS substrate for the considered analytes. For MG, the maximum values of RSD at the Raman bands 1172 cm^{-1}, 1398 cm^{-1}, and 1618 cm^{-1} were found to be 5.31%, 6.23%, and 5.57%, respectively, while for R6G these values at 770 cm^{-1}, 1362 cm^{-1}, 1510 cm^{-1} were found to be at 6.39%, 4.78% ,and 5.91%, respectively. The low RSD values of signal intensities, again infers a high reproducibility characteristic of the proposed SERS substrate.

4.3.5 Estimation of EF

EF of the proposed Cu-Au-ITO SERS substrate was calculated using equation 2.2 following the process described in section 2.3.4. The estimation of EF were illustrated in table 4.2.

Table 4.3 compares the performance of the current sensing system with some of the previously reported works on Cu-Au-ITO glass based SERS substrate for sensing of different analytes.

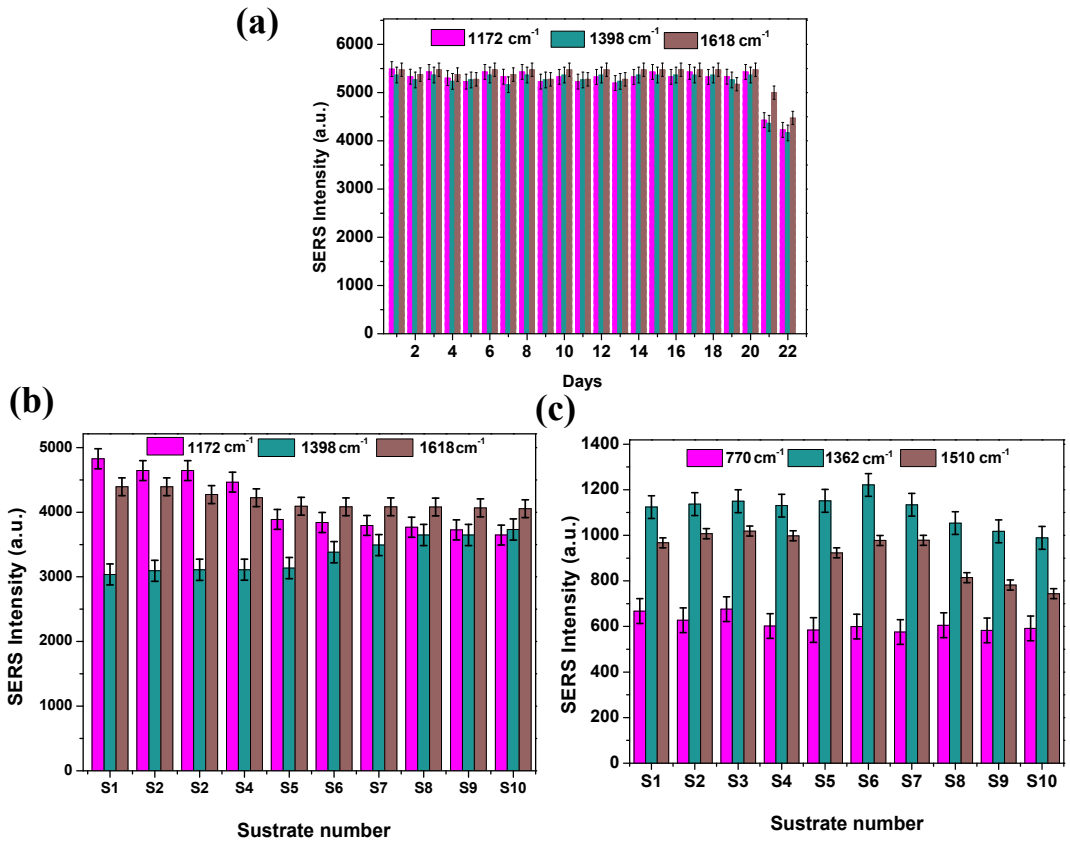

Figure 4.6: (a)Fluctuation of the SERS signal intensities with time. (b) Reproducibility characteristics of MG for ten identical substrates. (c) Reproducibility characteristics of R6G for ten identical substrates (Error bars are plotted using the standard deviation, calculated from five repetitions for each sample)

Table 4.2: Estimation of EF

Analyte	Signature Peak	I_{SERS}	I_{REF}	N_{SERS}	N_{REF}	EF
MG	1172 cm^{-1}	5500 a.u	500 a.u.	28.137	1.32×10^7	2.34×10^6
R6G	1362 cm^{-1}	852 a.u.	220 a.u	19.32		1.97×10^7

4.3.6 SERS analysis of SFZ and TCH

Upon noticing its performance on standard Raman active sample, the designed SERS platform has been used for sensing of the two antibiotics - SFZ and TCH. As shown in figure 4.7(a), the SERS spectra of SFZ are slightly varies from its normal Raman spectra which can be attributed to the binding of the analyte molecules to the surface of Cu-AuNPs, resulting in the enhancement of the Raman bands near 780 cm^{-1} and 1600 cm^{-1} [21].

To investigate the variations SERS signal intensities with the concentration of the analyte, samples of different concentrations were synthesized by adding proportionate amount of DI water in the stock sample. Figure 4.7(b) depicts the characteristic Raman spectra of SFZ for four different samples of concentrations 10 ppm, 1 ppm,

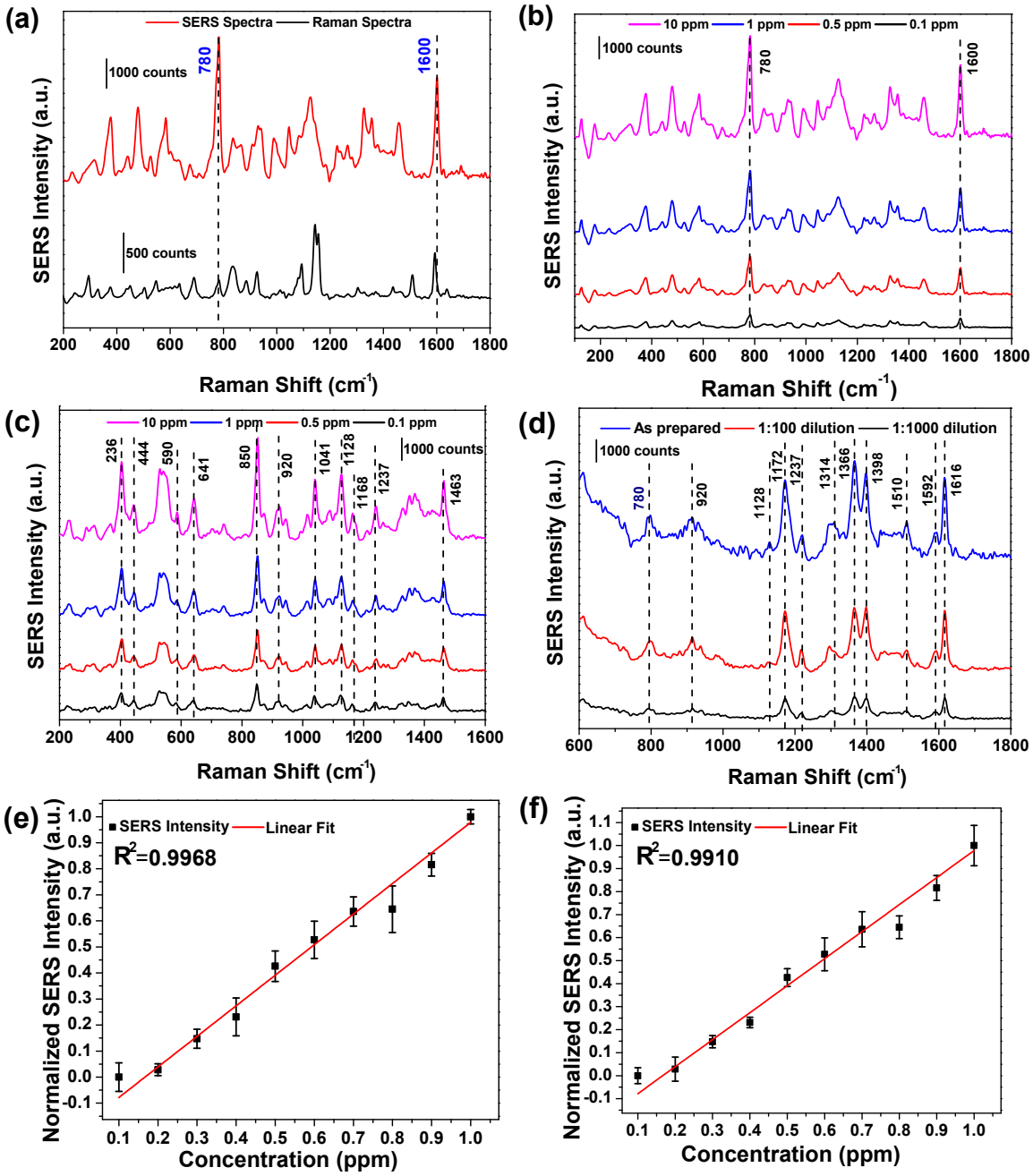

Figure 4.7: (a) Comparison of the SERS and normal Raman spectra of the SFZ. (b) Comparison of the SERS spectra of SFZ in four different concentrations. (c) Comparison of the SERS spectra of TCH in four different concentration. (d) SERS spectra of the mixed samples of MG, R6G, SFZ and TCH with concentration of 1 µM (e) Variation of the normalized SERS signal intensity with the concentration in the range from 0.1 to 1 ppm for SFZ corresponding to the signature Raman band of 780 cm^{-1}. (f) Variation of the normalized SERS signal intensity with the concentration in the range from 0.1 to 1 ppm for TCH corresponding to the signature Raman band of 850 cm^{-1} (Error bars are plotted using the standard deviation, calculated from five repetitions for each sample)

Table 4.3: Comparison of the proposed Cu-Au-ITO glass sensing scheme with some already reported SERS-based sensing works based on ED techniques

Substrate	Analyte	EF	RSD (%)	LOD (M)	Reference
Ag nanostructures on ITO glass film by electrodeposition	R6G	Not specified	$\sim 28.8\%$	10^{-10}	[19]
Flower-like gold nanostructures electrodeposited on ITO glass	Dopamine	10^6	Not specified	10^{-7}	[20]
Au-Ag bimetallic nanodendrite	2-Naphthalenethiol	10^6	Not specified	Not specified	[10]
Cu-Au-ITO glass SERS substrate with ML classification	MG, R6G, SFZ, TCH	10^7	8%	0.75×10^{-9}	Present work

0.5 ppm, and 0.1 ppm. The signal intensities are observed to decrease with decreasing sample concentrations. Figure 4.7(e) shows the variations of normalized SERS signal intensities of SFZ for signature Raman peaks at 780 cm^{-1} of ten different samples with concentrations ranging from 0.1 to 1 ppm. A linear variation in SERS intensities with $R^2 = 0.9968$ has been noticed, indicating a good linearity characteristic of the proposed technique for the target analyte. The unknown concentration of SFZ can be estimated by using the following regression equation 4.1.

$$Y = (1.17405 \pm 0.03284)X + (0.19573 \pm 0.02032) \tag{4.1}$$

Again, figure 4.7(c) shows the characteristic Raman spectra recorded by spectrometer for four different concentrations of TCH were considered for analysis. The normalized scattered Raman signal intensity variations for ten different concentrations of TCH ranging from 0.1 ppm to 1.0 ppm are shown in figure 4.7(f). Again, a linear correlation between the SERS signal intensities and the sample concentrations has been noticed with $R^2 = 0.9910$. The unknown concentration can be estimated by employing the following regression equation 4.2.

$$Y = (1.1104 \pm 0.0528)X + (0.0903 \pm 0.0382) \tag{4.2}$$

The attributes of the Raman bands for both SFZ and TCH are provided in the appendix section (table 8.9 and table 8.10).

4.3.7 SERS analysis of mixed samples

To demonstrate multiplex analyte detection capability of the proposed SERS platform, mixed analytes containing MG, R6G, SFZ, and TCH have been prepared in the laboratory. A fixed concentration of 1 µM of each analyte was mixed to form the mixed sample. A sample volume of 10 µL has been dispensed over the SERS platform and the back-scattered Raman signals of the analytes were recorded by the Raman

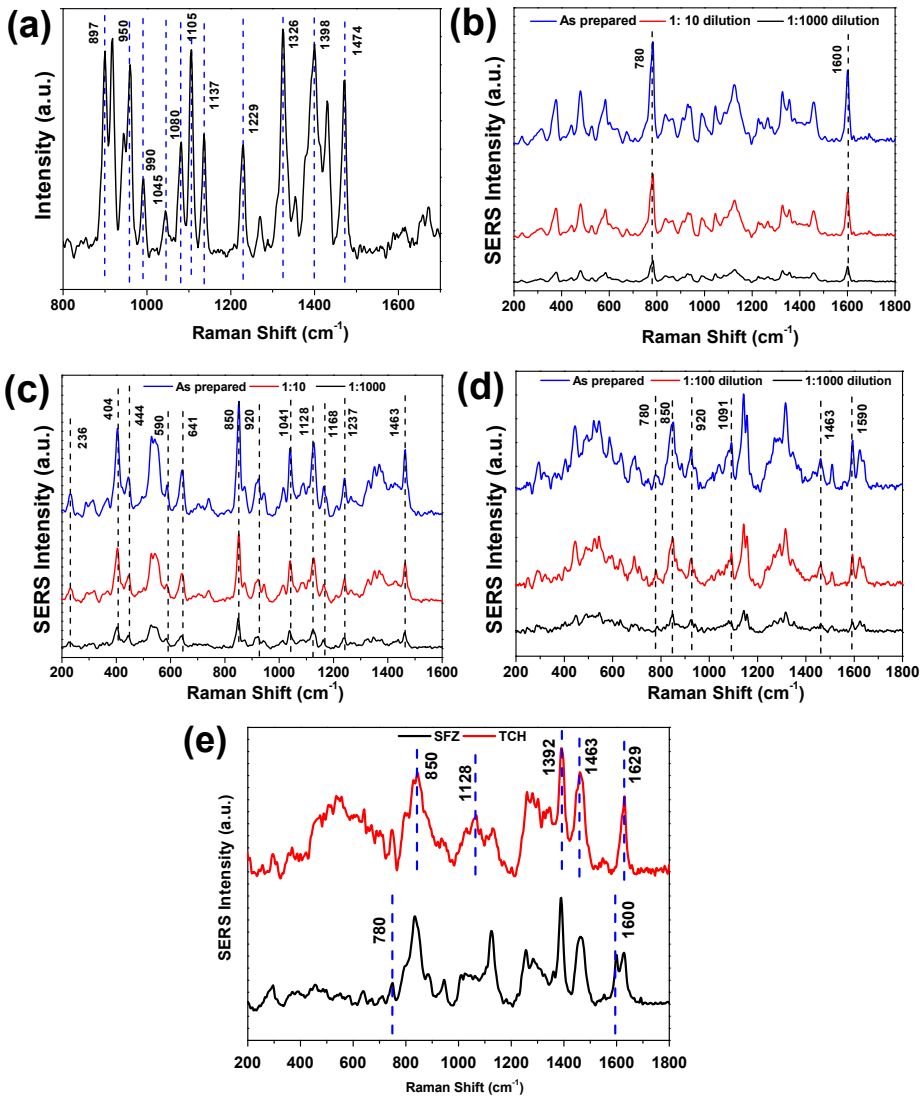

Figure 4.8: (a) Raman spectra of the background chemicals used in the sample extraction. (b) SERS spectra of the field-collected egg samples spiked with SFZ. (c) SERS spectra of the field collected egg samples spiked with TCH. (d) SERS spectra of the mixed SFZ and TCH in the ratio 1:1. (e) Interference study of the SFZ and TCH with oxytetracyline and enrofloxacin

spectrometer. Figure 4.8(d) shows the characteristic Raman spectra of the mixed sample recorded by the spectrometer at different dilution level. The Raman bands near 780 cm^{-1} and 1592 cm^{-1} confirm the presence of SFZ, while the bands near 920 cm^{-1}, 1128 cm^{-1}, and 1237 cm^{-1} confirm the presence of TCH; the rest of the peaks of TCH are found to be perturbed due to the presence of other analytes in the sample. Again, the characteristic Raman peaks near 1172 cm^{-1}, 1366 cm^{-1}, 1398 cm^{-1}, and 1616 cm^{-1} confirm the presence of MG in the mixed sample and the Raman bands near 1314 cm^{-1} and 1510 cm^{-1} are attributed to the presence of R6G in the mixed sample. For R6G, the other Raman bands are found to be perturbed due to the other analytes present in the mixed sample. The Raman bands near 780 and 1600 confirm the presence of SFZ in the extracted mixed sample and the signature Raman peaks

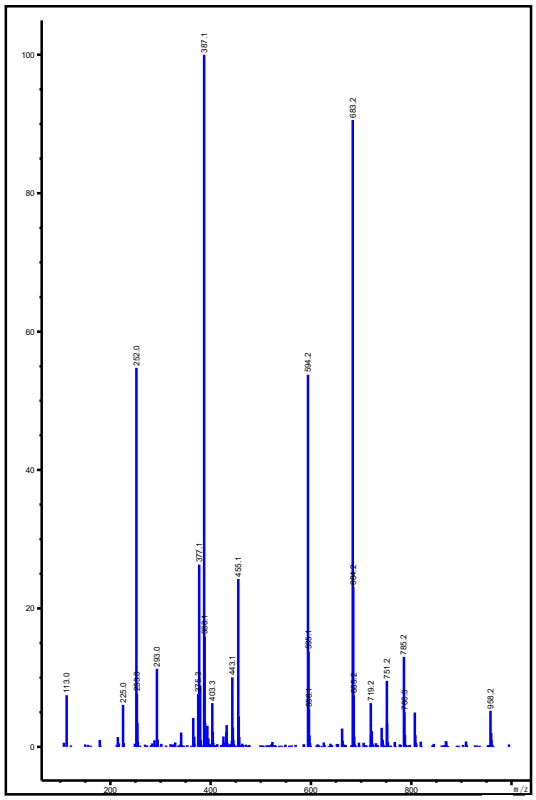

Figure 4.9: Mass spectra of the sample upon spiking with SFZ and TCH

at 850 cm^{-1}, 920 cm^{-1}, 1091 cm^{-1}, and 1463 cm^{-1} confirm the presence of TCH in the extracted mixed sample. From figure 4.8(d), it is evident that some peaks are observed to be perturbed when the SFZ and TCH are present in the mixed form. In a mixed media, the presence of one analyte influences the Raman bands of the other. The viability of the proposed sensing modality has been demonstrated through the validation with LC-MS for the extracted spiked samples.

Figure 4.9 shows the MS data of the extracted samples while spiking the analytes SFZ and TCH with 0.5 ppm concentration. A comparison of the SERS-based sensing for SFZ and TCH in farm egg samples and the percentage recovery rates are provided in table 4.4. The percentage recovery is estimated following the equation 4.3

$$\%recovery = \frac{Estimated\ conc}{Added\ conc} \times 100 \tag{4.3}$$

4.3.8 Interference study

In the next step, the interference study of the present sensing scheme has been carried out by taking two plausible interfering molecules namely oxytetracyline and enrofloxacin in the sample. For this, a fixed concentration of 0.5 ppm of these interfering analytes have been added to TCH and SFZ to form another mixed sample

Table 4.4: Estimation of the recovery rate for SFZ and TCH

Analyte	Sample no	Added (ppm)	Estimated (ppm) (SERS)	Recovery (%)	RSD (%, n = 5)
SFZ	S1	0.5	0.43	86	6.693
	S2		0.49	98	
	S3		0.53	106	
	S4		0.51	102	
	S5		0.49	98	
TCH	S1	0.5	0.52	104	12.28
	S2		0.49	98	
	S3		0.58	116	
	S4		0.6	120	
	S4		0.48	96	

which was followed by recording of the Raman spectra of the sample from designed bimetallic SERS platform. The characteristic Raman peaks at 850 cm^{-1}, 1128 cm^{-1}, 1293 cm^{-1}, 1463 cm^{-1}, and 1629 cm^{-1} confirm the presence of TCH and the Raman bands near 780 cm^{-1} and 1600 cm^{-1} confirm the presence of SFZ in the sample. For higher concentration of the interfering molecules, the resultant SERS spectra from the samples were affected due to high intense Raman peaks at 1392 cm^{-1} attributed to the OH vibration present in the oxytetracycline.

4.3.9 Implementation of ML

In the final step of the present work, an ML classification model has been developed for rapid identification and classification of two antibiotics in egg samples. Prior to performing the ML, the dimension of the dataset was reduced by using PCA for 200 egg samples. In PCA, the directions of the maximum variances were chosen as the principal component (PC)s. In the present study, two PCs were selected for the reduction of the dataset. The obtained PCs were used as the input dataset for the classification models - SVM, KSVM, Naïve Bayes, and KNN, respectively. The input dataset was subsequently split into two sets: training data (75%, or 150 samples) and test data (25%, or 50 samples). Additionally, model parameters like percentage accuracy and AUC in the ROC curve were estimated to find the optimal algorithm for the current sensing scheme. The KNN classification plots for the training and test sets of data are shown in 4.10(a) and (b), respectively.

As shown in figure 4.10 (a) and (b), the two antibiotic samples can be recognized using the ML algorithm in conjunction with PCA suggesting a very low false positives of the technique. Figure 4.10(c) compares the accuracy rates of various ML methods employed in the current scheme. The KNN algorithm combined with PCA performs the best as a classification model for current sensing platform. The ROC characteristics of the KNN classifier are shown in 4.10 (d). For the present sensing work, the AUC is found to be 94% indicating a good classification model. The confu-

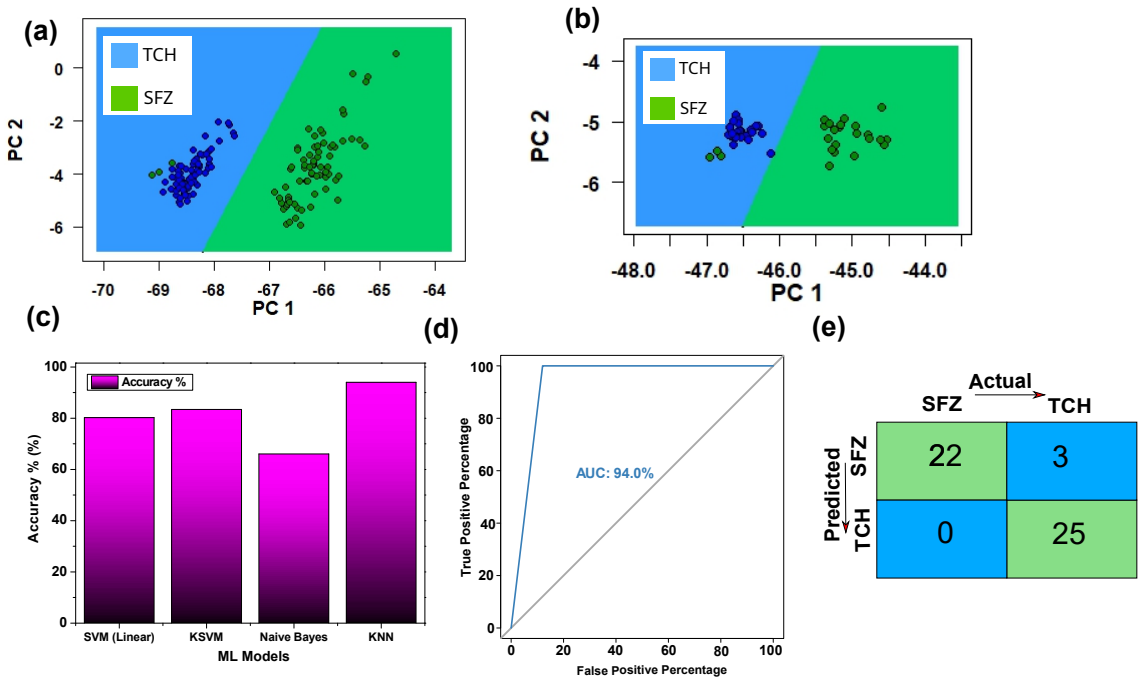

Figure 4.10: (a) ML classification plot using PCA-KNN for training set. (b) ML classification plot using PCA-KNN for test set. (c) Accuracy plot comparing the accuracies of the different ML modalities. (d) ROC curve for the PCA-KNN ML algorithm. (e) Confusion matrix obtained for the proposed sensing platform implementing PCA-KNN

sion matrix derived from the SVM classification model is shown in figure 4.10(e). In figure 4.10(e), the numbers in the blue segement display the inaccurate predictions while those in the green segment displays the accurate predictions. For a training set of 50 samples, the confusion matrix showed 47 correct predictions and 3 incorrect predictions.

The incorporation of bimetallic nanoparticles improves the electromagnetic field coupling at the site of the hotspot regions leading to an overall enhancement of the sensing performance. The synergistic interaction between CuNPs and AuNPs increases the electromagnetic hotspots on the surface of the SERS substrate and this has caused an overall enhancement in the Raman bands of the target analyte. Furthermore, the incorporation of bimetallic nanoparticles increases the stability compared to the monometallic counterparts. The fabrication process requires less than 5 min for the ED process, making it a viable approach for rapid fabrication of SERS substrate. The sensing of various antibiotics becomes a challenging when they are present in a complex matrix. The use of infrared laser ($\sim$ 785 nm) eliminates another possible source of interference namely the fluorescence emissions from the analyte.

4.4 Summary

The application of electrochemically deposited Cu-AuNPs on ITO glass substrate as a sensitive SERS platform has been explored. The process involves depositing CuNPs onto the ITO glass using the CA technique, followed by the deposition of AuNPs onto the Cu-ITO glass through CV employing a three-electrode system. The applicability of the proposed SERS platform has been demonstrated through detecting two commonly used antibiotics in the livestock industry. By following a selective sample extraction protocol, it is possible to expand the utility of the sensing scheme to other veterinary drugs. However, for more complex sample matrices, obtaining clear SERS signals might be challenging due to the presence of interfering molecules. Additionally, an ML classification model has been developed for classification of the targeted analytes from a mixed sample. An optimized model tailored for the current sensing setup enables quick identification of the analytes. Combining PCA with the KNN classifier a high classification accuracy was achieved for the present sensing platform.

References

[1] Radisic, A., Vereecken, P. M., Hannon, J. B., Searson, P. C., and Ross, F. M. Quantifying electrochemical nucleation and growth of nanoscale clusters using real-time kinetic data. *Nano letters*, 6(2):238–242, 2006.

[2] Lu, Y., Yuan, X., Jia, C., Lei, B., Zhang, H., Zhao, Z., Zhu, S., Zhao, Q., and Cai, W. Self-assembled bifunctional copper hydroxide/gold-ordered nanoarray composites for fast, sensitive, and recyclable SERS detection of hazardous benzene vapors. *Nanomaterials*, 13(13):2016, 2023.

[3] Zhang, J., Lu, S., Shi, G., Xie, W., Geng, Y., and Wang, Z. A study on a hybrid SERS substrates based on arrayed gold nanoparticle/graphene/copper cone cavities fabricated by a conical tip indentation. *Journal of Materials Research and Technology*, 22:1558–1571, 2023. Publisher: Elsevier.

[4] Xu, D., Wang, Z., Zhang, S., Zhang, Y., Yang, W., and Chen, J. Fabrication and SERS activity of high aspect ratio copper nanowires prepared via solid-state ionics method. *Physica E: Low-dimensional Systems and Nanostructures*, page 115789, 2023. Publisher: Elsevier.

[5] Chan, G. H., Zhao, J., Hicks, E. M., Schatz, G. C., and Van Duyne, R. P. Plasmonic properties of copper nanoparticles fabricated by nanosphere lithography. *Nano letters*, 7(7):1947–1952, 2007. Publisher: ACS Publications.

[6] Rivera-Rangel, R. D., Navarro-Segura, M. E., Arizmendi-Morquecho, A., and Sánchez-Domínguez, M. Electrodeposition of plasmonic bimetallic Ag-Cu nanodendrites and their application as surface-enhanced Raman spectroscopy (SERS) substrates. *Nanotechnology*, 31(46):465605, 2020. Publisher: IOP Publishing.

[7] Jones, T. Fabrication of nanostructured electrodes for electrochemical surface-enhanced Raman spectroscopy (E-SERS): a review. *Materials Science and Technology*, pages 1–15, 2023. Publisher: Taylor & Francis.

[8] Lindon, J. C., Tranter, G. E., and Koppenaal, D. *Encyclopedia of spectroscopy and spectrometry*. Academic Press, 2016.

[9] Clarke, O. J. R., Marie, G. J. H. S., and Brosseau, C. L. Evaluation of an electrodeposited bimetallic Cu/Ag nanostructured screen printed electrode for electrochemical surface-enhanced Raman spectroscopy (EC-SERS) investigations. *Journal of The Electrochemical Society*, 164(5):B3091, 2017. Publisher: IOP Publishing.

[10] Huan, T. N., Kim, S., Van Tuong, P., and Chung, H. AuAg bimetallic nanodendrite synthesized via simultaneous co-electrodeposition and its application as a SERS substrate. *RSC Adv.*, 4(8):3929–3933, 2014. ISSN 2046-2069. doi: 10.1039/C3RA44916E. URL http://xlink.rsc.org/?DOI=C3RA44916E.

[11] Sivanesan, A., Witkowska, E., Adamkiewicz, W., Dziewit, Ł., Kamińska, A., and Waluk, J. Nanostructured silver–gold bimetallic SERS substrates for selective identification of bacteria in human blood. *Analyst*, 139(5):1037–1043, 2014.

[12] Ralbovsky, N. M. and Lednev, I. K. Towards development of a novel universal medical diagnostic method: Raman spectroscopy and machine learning. *Chemical Society Reviews*, 49(20):7428–7453, 2020. Number: 20.

[13] Soman, K. P., Loganathan, R., and Ajay, V. *Machine learning with SVM and other kernel methods*. PHI Learning Pvt. Ltd., 2009.

[14] Dou, J., Dawuti, W., Li, J., Zhao, H., Zhou, R., Zhou, J., Lin, R., and Lü, G. Rapid detection of serological biomarkers in gallbladder carcinoma using fourier transform infrared spectroscopy combined with machine learning. *Talanta*, 259: 124457, 2023. Publisher: Elsevier.

[15] Ni, Y., Zhu, R., and Kokot, S. Competitive binding of small molecules with biopolymers: a fluorescence spectroscopy and chemometrics study of the interaction of aspirin and ibuprofen with BSA. *Analyst*, 136(22):4794–4801, 2011. Number: 22 Publisher: Royal Society of Chemistry.

[16] Medhi, A. and Mohanta, D. Deciphering Highly Sensitive Non-Enzymatic Glucose Sensor Based on Nanoscale CuO/PEDOT-MoS2 Electrodes in Chronoamperometry. *ECS Advances*, 1(4):046504, Oct. 2022. ISSN 2754-2734. doi: 10.1149/2754-2734/ac9324. URL https://dx.doi.org/10.1149/2754-2734/ac9324. Publisher: IOP Publishing.

[17] Wang, K., Lin, K., Huang, X., and Chen, M. A simple and fast extraction method for the determination of multiclass antibiotics in eggs using LC-MS/MS. *Journal of agricultural and food chemistry*, 65(24):5064–5073, 2017.

[18] R Core Team, R. R: A language and environment for statistical computing. 2013.

[19] Bian, J.-C., Chen, Z.-D., Li, Z., Yang, F., He, H.-Y., Wang, J., Tan, J. Z. Y., Zeng, J.-L., Peng, R.-Q., Zhang, X.-W., and others. Electrodeposition of hierarchical Ag nanostructures on ITO glass for reproducible and sensitive SERS application. *Applied Surface Science*, 258(17):6632–6636, 2012. Publisher: Elsevier.

[20] Bu, Y. and Lee, S. Flower-like gold nanostructures electrodeposited on indium tin oxide (ITO) glass as a SERS-active substrate for sensing dopamine. *Microchimica Acta*, 182:1313–1321, 2015. Publisher: Springer.

[21] Patze, S., Huebner, U., Liebold, F., Weber, K., Cialla-May, D., and Popp, J. SERS as an analytical tool in environmental science: the detection of sulfamethoxazole in the nanomolar range by applying a microfluidic cartridge setup. *Analytica chimica acta*, 949:1–7, 2017. Publisher: Elsevier.